An Illumination Model for a Skin Layer Bounded by Rough Surfaces

Jos Stam

Alias | wavefront
1218 Third Ave, 8th Floor,
Seattle, WA 98101

Abstract.
In this paper we present a novel illumination model that takes into account multiple anisotropic scattering in a layer bounded by two rough surfaces. We compute the model by a discrete-ordinate solution of the equation of radiative transfer. This approach is orders of magnitude faster than a Monte Carlo simulation and does not suffer from any noisy artifacts. By fitting low order splines to our results we are able to build analytical shaders. This is highly desirable since animators typically want to texture map the parameters of such a shader for higher realism. We apply our model to the important problem of rendering human skin. Our model does not seem to have appeared before in the optics literature. Most previous models did not handle rough surfaces at the skin's boundary. Also we introduce a simple analytical bidirectional transmittance distribution function (BTDF) for an isotropic rough surface by generalizing the Cook-Torrance model.

1   Introduction

This work was motivated by the desire to model the appearance of human skin. A good skin model has many obvious applications, notably in the entertainment industry, where virtual actors have to appear more life-like. Despite its importance this problem has only been marginally addressed in computer graphics. Traditional reflection models usually model the effects of subsurface scattering using a combination of a Lambert cosine term and an ambient term. Creating convincing pictures of human skin with these models is an art entirely left to the animator.

In this paper we propose a novel reflection model for a skin layer bounded by rough surfaces. Our model incorporates multiple anisotropic scattering within the skin layer. The only other model in computer graphics that is related to ours is the one proposed by Hanrahan and Krueger [5]. Their analytical model only handles skin layers bounded by perfectly smooth surfaces and they only account for single scattering. To handle multiple-scattering they use a Monte-Carlo simulation to precompute the distribution. In our experience the Monte Carlo method is too expensive to perform for all combinations of the values of the skin layer's parameters. Recently, Pharr and Hanrahan propose a generalization of the BRDF which takes into account volumetric scattering [18]. However, their technique still relies on an expensive Monte-Carlo simulation. This problem is adressed in recent work by Jensen et al. who use a diffusion approximation of the equation of radiative transfer to derive an analytical approximation for the reflection of light from a skin layer [8].

At first we expected to find an "off the shelf" solution from one of the related engineering fields. One such field, the medical sciences, studies the optics of skin for such applications as non-invasive surgery [23, 24]. Most research there either uses the

Monte Carlo method or a technique known as adding-doubling borrowed from the astronomy literature [20, 6]. Unfortunately, both techniques are too expensive for our purposes. Next we turned to the atmospheric sciences, where the reflection from the ocean is very close to that from a skin layer. There we found a very attractive model based on the discrete ordinate approximation of radiative transfer [3]. In particular, the work of Stamnes et al. solves the problem for a skin layer bounded by smooth surfaces [9, 21]. To handle rough surfaces the Monte Carlo is used [15]. We briefly mention that the discrete ordinate technique has been used in global illumination before [10, 12, 14].

Based on this extensive bibliographical search, we decided to extend Jin and Stamnes work to include rough surfaces. For this we first needed a good Bidirectional Transmittance Distribution Function (BTDF) model. We are aware of only one such model in computer graphics based on the wave theory of light [7]. Unfortunately this model is fairly complex, so we derive a simpler one in this paper for the first time. Our model is an extension of the BRDFs of Cook-Torrance [4] and of van Ginneken et al. [25]. Given the BRDF and the BTDF of the surfaces and the optical properties of skin we show how to efficiently solve the problem by a suitable "diagonalization" of the "transfer matrix." We use the machinery of Fourier transforms and eigenanalysis to perform this task. To build practical reflection models for computer graphics, we fit low-order splines to our discretized functions. Our approach is orders of magnitude faster than Monte Carlo methods, requires less memory, and does not suffer from any noisy artifacts.

The rest of the paper is organized as follows. The next section details the physics involved and introduces the equivalent discrete problem. In Section 3 we show how to solve the discrete problem efficiently. Section 4 presents a derivation of our BTDF. Section 5 clarifies many implementation issues and discusses the corresponding "skin shader". In Section 6 we present some results, while in Section 7 we conclude and discuss future research. Material of a rather technical nature is addressed in the appendices.

1.1 Notational Preliminaries

Much of the material in this paper can be presented more elegantly using a "matrix operator approach" [19]. Many relations are expressed more compactly without indices in vector and matrix form. In this paper all vectors are denoted by bold lowercase characters: $\mathbf{v}$. The elements of $\mathbf{v}$ are denoted by the corresponding italicized letter: v_i is the i-th component of $\mathbf{v}$. An element of a vector should not be confused with an indexed vector such as $\mathbf{v}_k$. A matrix is denoted by a bold upper case character such as $\mathbf{M}$ and its elements are denoted by $M_{i,j}$. The transpose of $\mathbf{M}$ is written $\mathbf{M}^T$.

2 Discretizing the Physics

2.1 Physical parameters

The basic physical quantity is the radiance u, which gives the amount of radiant power flowing from a particular position in a particular direction. Following Hanrahan and Krueger [5] we assume that the skin depth is along the z-direction and that the skin's properties are uniform in each xy-plane. We use the dimensionless optical depth $\tau = z/L$ instead of z, where L is the mean free path of a photon in the medium. Consequently, the radiance is a function of optical depth and direction. We represent a direction by an ordered pair $\pm\omega = (\pm\mu, \phi)$ where $\mu = \cos\theta$ is the cosine of the elevation angle θ and ϕ is the azimuthal angle (see Figure 1 (left)). In the following we always assume that the cosine $\mu \geq 0$. We therefore denote a downward direction by $-\omega = (-\mu, \phi)$. The use of the minus sign is purely notational in this context.
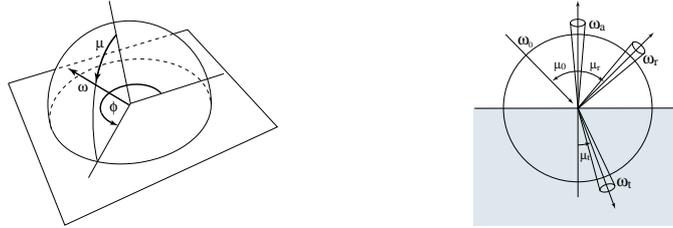
Fig. 1. Definition of a direction $\omega = (\mu, \phi)$ (left) and solid angles involved in a computing the reflection and refraction (right).
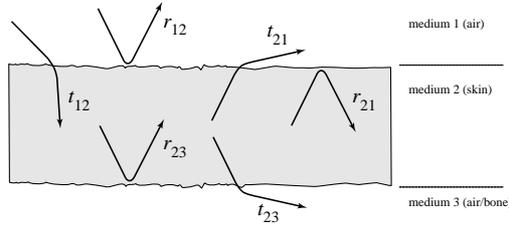
Fig. 2. Nomenclature for the BRDFs and BTDFs.

The optical properties of the skin are entirely modeled by its albedo Ω and its phase function p. The albedo gives the fraction of light that is scattered versus absorbed, while the phase function gives the probability that a photon travelling in a direction ω' is scattered in another direction ω. We rely on the *Henyey-Greenstein phase function*, a useful model frequently seen in the optics literature:

$$p(\omega', \omega) = \frac{1 - g^2}{(1 + g^2 - 2g \cos \gamma)^{3/2}}.$$

Here γ is the angle between the directions ω' and ω. The anisotropy factor $g \in [0, 1]$ models how much light is scattered forward. We associate with the phase function a linear scattering functional:

$$\mathcal{S}\{u\}(\tau, \omega) = \frac{\Omega}{4\pi} \int_{4\pi} p(\omega', \omega) u(\tau, \omega') \, d\omega', \tag{1}$$

where the integration is over all possible directions.

The reflection and refraction at the skin's boundaries are modeled as isotropic rough surfaces. In our model we assume that the skin has a uniform index of refraction n_2 and is bounded above and below by media having indices equal to n_1 and n_3, respectively. Both the transmission and reflection models depend on a roughness parameter σ. The BRDF and BTDF are denoted by $r_{ij}(\omega, \omega')$ and $t_{ij}(\omega, \omega')$, respectively, for light coming from material $i \in 1, 2, 3$ arriving at material $j \in 1, 2, 3$, where, for example, r_{12} models the reflection off of the top surface. This nomenclature is clarified in Figure 2. We associate with these distributions linear reflection and transmission operators:

$$\mathcal{R}_{ij}\{u\}(\tau, \pm\omega) \;\; = \;\; \int_{2\pi} r_{ij}(\mp\omega', \pm\omega) u(\tau, \mp\omega') \mu' \, d\omega', \tag{2}$$

$$\mathcal{T}_{ij}\{u\}(\tau, \pm\omega) = \int_{2\pi} t_{ij}(\pm\omega', \pm\omega)u(\tau, \pm\omega')\mu' \, d\omega', \tag{3}$$

where the integration is over the positive hemisphere and the signs depend on the BRDF or BTDF considered, e.g., r_{12} has opposite signs from r_{21} as is evident from Figure 2.

2.2 Equation of Transfer

An equation for the radiance within the skin is obtained by considering its variation in an infinitesimal cylinder aligned with the direction ω. The change is equal to the amount of light scattered into this direction minus the light absorbed and scattered out of this direction:

$$-\mu\frac{du}{d\tau} = -u + \mathcal{S}\{u\}, \tag{4}$$

where $\mathcal{S}$ is the scattering operator defined in Equation 1. To completely specify the problem, this equation requires boundary conditions at the top and the bottom of the skin layer. At the skin's surface ($\tau = 0$) the downwelling radiance is equal to the transmitted radiance plus the internal reflections of the radiance coming from the internal layer:

$$u(0, -\omega) = t_{12}(-\omega_0, -\omega) + \mathcal{R}_{21}\{u\}(0, -\omega). \tag{5}$$

Similarly, if we assume there are no sources below the skin, the upwelling radiance at the bottom of the layer ($\tau = \tau_b$) is given by

$$u(\tau_b, \omega) = \mathcal{R}_{23}\{u\}(\tau_b, \omega). \tag{6}$$

Once Equation 4 is solved using these boundary conditions, the BRDF and the BTDF due to scattering in the skin's layer are equal to

$$r_s(-\omega_0, \omega) = \mathcal{T}_{21}\{u\}(0, \omega)/\mu_0 \quad \text{and} \quad t_s(-\omega_0, -\omega) = \mathcal{T}_{23}\{u\}(\tau_b, -\omega)/\mu_0,$$

respectively. In addition, the reflection due to an ambient light source of radiance is modeled by integrating the skin's BRDF over all incident directions $-\omega_0$:

$$r_a(\omega) = \int_{2\pi} r_s(-\omega_0, \omega) \, \mu_0 \, d\mu_0.$$

The total amount of light reflected off the skin is the sum of the part directly reflected by the surface, the ambient term and the radiance leaving the subsurface layer:

$$r_{tot}(\omega) = r_{12}(-\omega_0, \omega) + r_a(\omega) + r_s(-\omega_0, \omega).$$

In Section 4 we provide a model for r_{12} (and the other r_{ij} and t_{ij}) while the next section describes a method of solution for r_s and t_s.

2.3 Angular Discretization

We discretize the angular part of Equation 4 in two steps. Because we assume that the surface roughness is isotropic and that the skin is horizontally uniform, we can decompose the azimuthal dependence of the radiance into a cosine series:

$$u(\tau, \omega) = \sum_{k=0}^{N} u_k(\tau, \mu) \cos k(\phi - \phi_0). \tag{7}$$

Next we discretize the cosines μ into $2M$ discrete samples (see Appendix A for how they are chosen):

$$\mu_1, \mu_2, \cdots, \mu_M, -\mu_1, -\mu_2, \cdots, -\mu_M. \tag{8}$$

These values are also known as "ordinates," hence the name "discrete-ordinates" to refer to this type of discretization. The corresponding values of the discretized radiances are stored in a $2M$ vector

$$\mathbf{u}_k(\tau) = (u_k(\tau, \mu_1), \cdots, u_k(\tau, -\mu_M))^T \qquad k = 0, \cdots, N.$$

As shown in Appendix A, the scattering operator in Equation 4 is discretized into a collection of $N+1$ matrices $\mathbf{S}_k$ ($k = 0, \cdots, N$), each of size $2M \times 2M$. These discretizations convert the transfer equation into $N+1$ decoupled linear ordinary differential vector equations:

$$-\mathbf{W}\frac{d\mathbf{u}_k(\tau)}{d\tau} = -\mathbf{u}_k(\tau) + \mathbf{S}_k\mathbf{u}_k(\tau),$$

where $\mathbf{W}$ is a diagonal matrix containing the samples of Equation 8. The last equation can be written more compactly as

$$\frac{d\mathbf{u}_k(\tau)}{d\tau} = \mathbf{M}_k\mathbf{u}_k(\tau), \tag{9}$$

where $\mathbf{M}_k = \mathbf{W}^{-1}(\mathbf{I} - \mathbf{S}_k)$ and $\mathbf{I}$ is the identity matrix. Equation 9 is the main equation of this paper. In the next section we show how to solve it efficiently.

3 Direct Solution of the Discrete Problem

This section is inspired by the work of Jin and Stamnes [9]. However, our compact vector/matrix notation greatly simplifies the presentation. Our approach is also more general, since we consider surfaces of arbitrary roughness at the boundaries.

3.1 Diagonalization

We assume that the skin is composed of a layer with constant optical properties sandwiched between two isotropic rough surfaces. In order to simplify the notation in this section, we will drop the dependence of all quantities on the index "k". This is justified because the equations for different terms in the cosine expansion are entirely decoupled. In the skin the radiance satisfies the following equation:

$$\frac{d\mathbf{u}(\tau)}{d\tau} = \mathbf{M}\mathbf{u}(\tau).$$

Ignoring the boundary conditions for the moment, we see that this is a homogeneous vector ordinary differential equation. Such an equation is solved efficiently by putting the matrix $\mathbf{M}$ into diagonal form. Indeed, in diagonal form the equations are decoupled and can be solved analytically. Diagonalizing $\mathbf{M}$ is equivalent to computing its eigenvalues and eigenvectors: $\mathbf{M} = \mathbf{V}\mathbf{L}\mathbf{V}^{-1}$. Here $\mathbf{L}$ is a diagonal matrix containing the eigenvalues of $\mathbf{M}$:

$$\mathbf{L} = \text{diag}(\lambda_1, \cdots, \lambda_M, -\lambda_1, \cdots, -\lambda_M)$$

where $\lambda_i > 0$ for $i = 1, \cdots, M$ and $\mathbf{V}$ contains the eigenvectors stored columnwise. If we let $\mathbf{w}(\tau)$ be the transformed radiance $\mathbf{w} = \mathbf{V}^{-1}\mathbf{u}$, then

$$\frac{d\mathbf{w}(\tau)}{d\tau} = \mathbf{L}\mathbf{w}(\tau).$$

The exact solution to this differential equation is given by:

$$\mathbf{w}(\tau) = e^{\mathbf{L}\tau}\mathbf{u}_0, \tag{10}$$

where the exponential is simply the diagonal matrix whose elements are the exponential of the elements of $\mathbf{L}\tau$. The vector $\mathbf{u}_0$ in Equation 10 is to be determined from the boundary conditions. The radiance in the layer is then obtained by inverting our earlier transformation:

$$\mathbf{u}(\tau) = \mathbf{V}\mathbf{w}(\tau) = \mathbf{V}e^{\mathbf{L}\tau}\mathbf{u}_0. \tag{11}$$

Our next step is to find a vector $\mathbf{u}_0$ satisfying the boundary conditions.

3.2 Solving the Discrete Problem: Boundary conditions

We have just shown that the radiance in each layer can be solved for directly in terms of the eigenvectors and eigenvalues of the transfer matrix. We can rewrite Equation 11 separating the parts corresponding to upward and downward directions:

$$\left(\begin{array}{c} \mathbf{u}^+(\tau) \\ \mathbf{u}^-(\tau) \end{array} \right) = \left(\begin{array}{cc} \mathbf{V}^+ & \mathbf{V}^- \\ \mathbf{V}^- & \mathbf{V}^+ \end{array} \right) \left(\begin{array}{c} \mathbf{E}(\tau)\mathbf{u}_0^+ \\ \mathbf{E}(-\tau)\mathbf{u}_0^- \end{array} \right), \tag{12}$$

where each of the matrices $\mathbf{E}(t) = e^{\mathbf{L}^+ t}$ contains half of the exponentials. The goal in this section is to compute the unknown vectors $\mathbf{u}_0^+$ and $\mathbf{u}_0^-$ given by Equations 5 and 6. First, let $\mathbf{R}_{ij}$ and $\mathbf{T}_{ij}$ denote the discrete versions of $\mathcal{R}_{ij}$ and $\mathcal{T}_{ij}$ respectively. Since they are defined only over the positive hemisphere they are of size $M \times M$. The top and bottom boundary conditions in terms of these matrices are

$$\mathbf{u}^-(0) = \mathbf{T}_{12}\mathbf{d}_0 + \mathbf{R}_{21}\mathbf{u}^+(0) \quad \text{and} \tag{13}$$

$$\mathbf{u}^+(\tau_b) = \mathbf{R}_{23}\mathbf{u}^-(\tau_b). \tag{14}$$

The vector $\mathbf{d}_0$ represents the incident radiances, and for a directional light source is zero for each entry except for the entry corresponding to $-\mu_0$ where it is equal to one. By substituting Equations 13 and 14 into Equation 12 and rearranging,

$$\left(\begin{array}{cc} \mathbf{V}^- - \mathbf{R}_{21}\mathbf{V}^+ & \mathbf{V}^+ - \mathbf{R}_{21}\mathbf{V}^- \\ \left(\mathbf{V}^+ - \mathbf{R}_{23}\mathbf{V}^-\right)\mathbf{E}(\tau_b) & \left(\mathbf{V}^- - \mathbf{R}_{23}\mathbf{V}^+\right)\mathbf{E}(-\tau_b) \end{array} \right) \left(\begin{array}{c} \mathbf{u}_0^+ \\ \mathbf{u}_0^- \end{array} \right) = \left(\begin{array}{c} \mathbf{T}_{12}\mathbf{d}_0 \\ \mathbf{0} \end{array} \right).$$

This system, however, is ill-conditioned because the matrix $\mathbf{E}(\tau_b)$ has entries that grow exponentially with τ_b. Fortunately, we can easily fix this problem by setting $\mathbf{u}_0^+ = \mathbf{E}(-\tau_b)\tilde{\mathbf{u}}_0^+$ and solving for $(\tilde{\mathbf{u}}_0^+, \mathbf{u}_0^-)$ instead [21]. The new system becomes:

$$\left(\begin{array}{cc} \left(\mathbf{V}^- - \mathbf{R}_{21}\mathbf{V}^+\right)\mathbf{E}(-\tau_b) & \mathbf{V}^+ - \mathbf{R}_{21}\mathbf{V}^- \\ \mathbf{V}^+ - \mathbf{R}_{23}\mathbf{V}^- & \left(\mathbf{V}^- - \mathbf{R}_{23}\mathbf{V}^+\right)\mathbf{E}(-\tau_b) \end{array} \right) \left(\begin{array}{c} \tilde{\mathbf{u}}_0^+ \\ \mathbf{u}_0^- \end{array} \right) = \left(\begin{array}{c} \mathbf{T}_{12}\mathbf{d}_0 \\ \mathbf{0} \end{array} \right). \tag{15}$$

This linear system is well behaved and can be solved using any standard linear solver. Once the solution is obtained, the upward radiance at the top and the downward radiance at the bottom of the layer are given by:

$$\mathbf{u}^+(0) = \mathbf{V}^+\mathbf{E}(-\tau_b)\tilde{\mathbf{u}}_0^+ + \mathbf{V}^-\mathbf{u}_0^- \quad \text{and} \quad \mathbf{u}^-(\tau_b) = \mathbf{V}^-\tilde{\mathbf{u}}_0^+ + \mathbf{V}^+\mathbf{E}(-\tau_b)\mathbf{u}_0^-,$$

respectively. These are the radiances just inside the rough surfaces of the skin layer. To compute the radiances exiting the surface, we have to multiply these radiances by the transmission matrices $\mathbf{T}_{21}$ and $\mathbf{T}_{23}$, respectively:

$$\mathbf{u}_r = \mathbf{T}_{21}\mathbf{u}^+(0) \quad \text{and} \quad \mathbf{u}_t = \mathbf{T}_{23}\mathbf{u}^-(\tau_b). \tag{16}$$

ComputeRT:
    For $k = 0, \cdots, N$ do
        Compute the scattering matrix $\mathbf{M}_k$ (Appendix A)
        Compute the reflection and transmission matrices $\mathbf{R}_{ij}$ and $\mathbf{T}_{ij}$ (Appendix D)
        Compute eigenstructure of $\mathbf{M}_k$
        For $i = 1, \cdots, M$
            Solve linear system for incoming direction μ_i (Equation 15)
            Transmit radiances out of the layer (Equation 16)
            Set the i-th columns of $\mathbf{R}_k$ and $\mathbf{T}_k$
        next
    next

Fig. 3. Summary of our algorithm.

3.3 Summary

First we restore the subscript "k" to indicate that the radiances of Equation 16 correspond to a single term in the cosine series. Consequently, the complete description of the radiances is given by the following vectors

$$\mathbf{u}_{r,0}, \cdots, \mathbf{u}_{r,N} \quad \text{and} \quad \mathbf{u}_{t,0}, \cdots, \mathbf{u}_{t,N}.$$

These radiances are for a particular incoming direction $-\omega_0 = (-\mu_0, 0)$. To get a discrete description of the BRDF r_s of the skin layer we sample the incoming directions at the ordinates $\mu_1, \cdots, \mu_M$. The discrete representation of the BRDF is, therefore, a collection of $N + 1$ matrices $\mathbf{R}_k$ of size $M \times M$ ($k = 0, \cdots, N$). The i-th column of this matrix consists of the vector $\mathbf{u}_{r,k}$ computed for the incident direction $(-\mu_i, 0)$, $i = 1, \cdots, M$. In a similar fashion we build a set of matrices $\mathbf{T}_k$ for the BTDF t_s of the skin layer ($k = 0, \cdots, N$). A high level description of the algorithm that computes these matrices is given in Figure 3.

    We have precomputed these matrices for different values of the parameters that model the skin layer. These parameters are the transparency $T = e^{-\tau_b}$, the albedo Ω, the anisotropy factor g of the phase function, and the roughness σ of the surfaces bounding the skin layer. Each parameter is dimensionless and takes on values between zero and one. The ratio of the indices of refraction is kept constant throughout: it is set to 1.4, roughly that of human skin. The number of ordinates M was determined from the discretizations of the BRDF and the BTDF of the skin's surface (derived in the next section). For a roughness $\sigma = 0.1$ we nededed $M = 30$ ordinates while for other values $M = 24$ was sufficient. The number of cosine series is always set to twice the number of ordinates: $N = 2M$ [9].

    Because the scattering matrix depends only on Ω and g, we first computed the eigenstructures for a set of values of the parameters. We used the RG routine from EISPACK [17] to compute the eigenvectors and eigenvalues. We encountered no numerical problems except when the albedo was exactly one. An easy fix is simply to set the albedo to a value almost equal to one, i.e., $\Omega = 0.999999$. Once the eigenstructures were available we used them to precompute the reflection r_s and transmission t_s of the skin layer. We used the routine DGESL from LINPACK to solve the linear system of Equation 15.

    The precomputation generates a huge data set. Our next task was to compress the data using well chosen approximations. We first experimented with the elegant non-linear representation of Lafortune et al. [11]. We did get some good matches using three cosine lobes. However, in many cases the non-linear least square solver got stuck
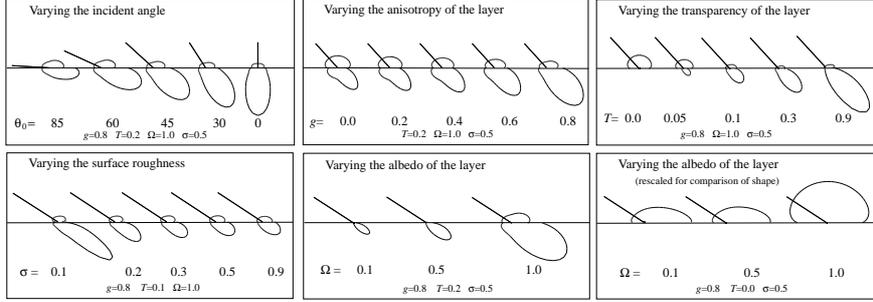
Fig. 4. Cross-sections of the reflection and transmission functions of the skin layer for different values of the parameters.

in local minima. For these reasons we adopted a less efficient but more straightforward compression scheme. First, not all cosine terms need to be included. For the reflection at the top of the layer we found that in general, 5 terms ($N = 4$) were sufficient, while for the transmission at the bottom 15 ($N = 14$) terms were required. These numbers were obtained by visually comparing the data to the approximation. We further compressed the data by fitting a cubic Bezier surface to the data stored in the reflection (resp. transmission) matrix $\mathbf{R}_k$ (resp. $\mathbf{T}_k$). We constrained the control vertices to respect the symmetry of these matrices (Helmholtz reciprocity).

In Figure 4 we demonstrate the effect of our parameters on the reflection and transmission functions. The simple shapes of the lobes first led us to believe that they might be modeled by simple analytical expressions. The variation with each parameter is, however, quite subtle and none of our analytical estimations could handle all variations at the same time. Analytical solutions are rare when multiple scattering is included. Even the simplest case of a semi-infinite constant medium with isotropic scattering does not admit an analytical solution [3]. The distributions are clearly different from a simple constant Lambert term. The simple analytical model of Hanrahan and Krueger is recovered for low albedos and smooth surfaces.

4   Reflection and Refraction from Rough Surfaces

The derivation of our BRDF and BTDF models follows the work of van Ginneken et al. [25]. We assume that our surface is an isotropic gaussian random height field [1]. The probability that a normal ω_a lies within an infinitesimal solid angle $d\omega_a = (d(\cos\theta_a), d\phi_a)$ is given by the Beckmann function [1]:

$$P(\omega_a)\ d\omega_a = \frac{1}{2\pi\sigma^2\cos^3\theta_a}\exp\left(-\frac{\tan^2\theta_a}{2\sigma^2}\right)\ d\omega_a, \qquad (17)$$

where σ is the RMS slope of the surface. Let the surface be illuminated by a directional source of irradiance E_0 of direction $\omega_0 = (\cos\theta_0, \phi_0)$. For each direction ω_r, resp. ω_t, there is a unique normal ω_a that will reflect (resp. refract) the incoming light in the direction ω_r (resp. ω_t).

The incoming power at a surface element dA with normal ω_a is equal to:

$$\Phi_0 = E_0\ \cos\theta_0'\ dA,$$

where $\cos\theta_0'$ is the cosine of the angle between the normal and the incoming direction. The amount of power that is reflected and refracted is determined by the Fresnel factor $F(\cos\theta_0', \eta)$ [2], where η is the ratio of indices of refraction. Indeed, a fraction F of the power is reflected while a portion $(1 - F)$ is refracted. To get the total radiance reflected into direction ω_r, we multiply the radiance reflected by a point of the surface with normal ω_a by the Beckmann probability function defined in Equation 17:

$$u_r = \frac{F\ E_0\ \cos\theta_0'\ P(\omega_a)\ d\omega_a}{\cos\theta_r d\omega_r}.$$

The solid angles $d\omega_r$ and $d\omega_a$ are not independent. This can be understood intuitively: by varying the normal in the cone $d\omega_a$ we get a corresponding variation around the reflected direction ω_r. The size of this variation is exactly the factor which relates the two solid angles. The precise relation between them was cited by Torrance and Sparrow [22]:

$$d\omega_r = 4\cos\theta_0'\ d\omega_a.$$

Nayar provides an elegant geometric proof of this result [16]. In Appendix B we give an alternative proof which easily generalizes to the case of refraction to be discussed below. Consequently, our BRDF is:

$$r = \frac{F(\cos\theta_0', \eta)\ P(\omega_a)}{4\ \cos\theta_r\ \cos\theta_0}.$$

We now derive the BTDF in a similar fashion. As in the reflected case, the total radiance refracted into a direction ω_t is given by:

$$u_t = \frac{(1 - F)\ E_0\ \cos\theta_0'\ P(\omega_a)\ d\omega_a}{\cos\theta_t\ d\omega_t}.$$

The relation between the solid angles $d\omega_t$ and $d\omega_a$ is, however, very different. At first we did not pay too much attention to this relationship and simply assumed $d\omega_a = d\omega_t$. But when we compared our analytical model with a Monte Carlo simulation for validation, we found large discrepancies. Finally, after a careful analysis of other BRDF derivations [4, 25] we realized the importance of this relation. In Appendix B we prove that:

$$d\omega_t = \frac{(\cos\theta_0' - \mu_t)^2}{\eta\mu_t}\ d\omega_a = G(\cos\theta_0', \eta)\ \cos\theta_0'\ d\omega_a,$$

where $\mu_t = \sqrt{\cos\theta_0' + \eta^2 - 1}$. With this factor our BTDF is:

$$t = \frac{(1 - F(\cos\theta_0', \eta))\ P(\omega_a)}{\cos\theta_t \cos\theta_0\ G(\cos\theta_0', \eta)}.$$

We also multiply this function by the shadowing function proposed by van Ginneken et al. [25]. We prefer this shadowing function over the one used by Cook and Torrance [4] since it is consistent with the underlying model for the surface.

The BRDF and the BTDF are shown for different ratios of indices of refraction η and roughness values σ in Figure 5. The top figure corresponds to a ratio $\eta = 1.4$ which is that of skin. These plots correspond to the functions r_{12}, t_{12}, r_{21} and t_{21} of our skin model. As mentioned above we have validated our derivation using a Monte Carlo simulation. Whether this provides a good model for rough surfaces will have to be settled by experiment. At least, Cook and Torrance reported good agreement with experiment for the function r_{12} [4].
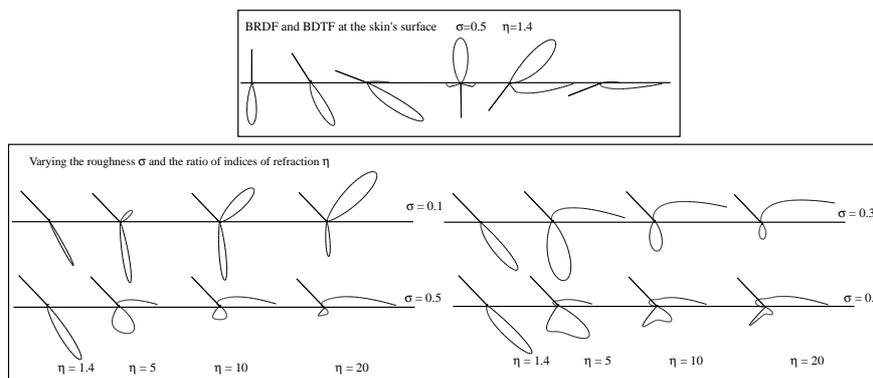
Fig. 5. Our new BRDFs and BTDFs for a rough surface. The distributions are rescaled to fit in the figure.

5 The Skin Shader

We have implemented our reflection model as a shader plugin in our animation software MAYA. The plugin is available for free on our company's web page[1]. The web page also provides more information on the parameters of our skin shader. Several of our customers have recently started to use our shader in production with good results.

Figure 6 shows several examples of human heads rendered using our new skin shader. Figure 6.(a) compares our model (right) to a Lambert shader (left) and the Hanrahan-Krueger (HK) model (center). Our model seems to be a blend between these two models, which is consistent with the plots in Figure 4. Unfortunately, the comparison is necessarily very vague. Indeed, we manually tried to find a set of parameters for both the Lambert shader and the HK model which was as close as possible to our results. In particular, we had to "brighten up" the HK model since it assumes single-scattering. Figure 6.(b) shows our model illuminated by different area light sources. Notice also that we texture mapped both the albedo and the roughness of the lips. Figure 6.(c) is similar for a male head. Finally 6.(d) demonstrates another application of our shader (notice that the surfaces have been bump mapped).

6 Conclusions and Future Work

This paper presented a novel analytical model for the reflection and transmission of light from a skin layer bounded by rough surfaces. The model includes the effects of multiple anisotropic scattering within the skin. To the best of our knowledge a model of this generality has not appeared before in the optics literature.

Our model currently lacks any form of experimental validation. The differences between our model and a simple Lambert shader are not as dramatic as we had expected. The difference is, however, noticeable. We hope to compare our model to the Cornell data [13] and possibly to other data sets from other related disciplines. Also we hope to find a better compression scheme for our computed data, most likely a simple analytical model with a few parameters which can be fit using a non-linear optimization technique.

---

[1] http://www.aliaswavefront.com by following "community" and "Download".

Acknowledgments

A   Details: Angular Discretization

In this appendix we provide the missing details of Section 2.3 that lead to explicit expressions for the matrices $\mathbf{M}_k$.

First, we expand the phase function into a cosine series as well:

$$p(\omega', \omega) = \sum_{k=0}^{N} p_k(\mu', \mu) \cos k(\phi - \phi'), \tag{18}$$

where the p_k are functions of the anisotropy factor g and the associated Legendre functions as shown in Appendix C. If we substitute Equations 7 and 18 into Eq. 4 we get the following $N + 1$ equations ($k = 0, \cdots, N$):

$$\mu \frac{d}{d\tau} u_k(\mu) = u_k(\mu) - \Omega_k \int_{-1}^{+1} p_k(\mu', \mu) \, u_k(\mu') \, d\mu', \tag{19}$$

where $\Omega_k = \Omega \frac{(1+\delta_{0,k})}{4}$ and $\delta_{i,j}$ is the Kronecker symbol. We now discretize the problem further by approximating the integrals in Equations 19 using a quadrature:

$$\int_{-1}^{+1} f(\mu') \, d\mu' \approx \sum_{m=1}^{M} w_m \left\{ f(-\mu_m) + f(\mu_m) \right\},$$

where w_m are the weights and $\mu_m \geq 0$ are the ordinates of the quadrature. With this approximation Equation 19 becomes a set of linear equations:

$$\mu_n \frac{d}{d\tau} u_k(\mu_n) = u_k(\mu_n) - \Omega_k \sum_{m=1}^{M} w_m \left\{ p_k(-\mu_m, \mu_n) u_k(-\mu_m) + p_k(\mu_m, \mu_n) u_k(\mu_m) \right\}$$

$$-\mu_n \frac{d}{d\tau} u_k(-\mu_n) = u_k(-\mu_n) - \Omega_k \sum_{m=1}^{M} w_m \left\{ p_k(-\mu_m, -\mu_n) u_k(-\mu_m) + p_k(\mu_m, -\mu_n) u_k(\mu_m) \right\}.$$

Since $p_k(-\mu_m, \mu_n) = p_k(\mu_m, -\mu_n)$ and $p_k(\mu_m, \mu_n) = p_k(-\mu_m, -\mu_n)$ we introduce the following two $M \times M$ matrices:

$$\begin{aligned}
(A_k)_{n,m} &= (\Omega_k w_m p_k(\mu_m, \mu_n) - \delta_{n,m})/\mu_n \quad \text{and} \\
(B_k)_{n,m} &= \Omega_k w_m p_k(-\mu_m, \mu_n)/\mu_n.
\end{aligned}$$

Consequently, recalling the vector notations introduced in Section 2.3:

$$\mathbf{M}_k = \begin{pmatrix} -\mathbf{A}_k & -\mathbf{B}_k \\ \mathbf{B}_k & \mathbf{A}_k \end{pmatrix}.$$

B Relating $d\omega$ to $d\omega_a$

Computing the relationship between the two differentials $d\omega_a$ and $d\omega$ is mathematically equivalent to computing the Jacobian of the change of coordinates $\omega_a \to \omega$. In this appendix we compute the Jacobians for both the reflected and the refracted solid angles. We compute the change of coordinates in three steps:

$$\omega_a \longrightarrow (x_a, y_a) \longrightarrow (x, y) \longrightarrow \omega.$$

The relation between the spherical and cartesian coordinates is well known and given by

$$dx_a \, dy_a = \mu_a \, d\omega_a \quad \text{and} \quad dx \, dy = \mu \, d\omega.$$

Following the approach of Nayar et al. [16] we assume without loss of generality that the solid angle of the normal $d\omega_a$ is centered along the normal $(0, 0, 1)$. We also assume that the source is coming from the direction $(\mu_0, 0)$, or in cartesian coordinates $\mathbf{v}_0 = (\sqrt{1 - \mu_0^2}, 0, \mu_0)$. See Figure 1 (right). Let

$$\mathbf{n}(x_a, y_a) = (x_a, y_a, \sqrt{1 - x_a^2 - y_a^2})$$

be a normal in $dx_a \, dy_a$. Then the reflected and refracted directions are equal to

$$
\begin{aligned}
\mathbf{r} &= 2(\mathbf{n} \cdot \mathbf{v}_0)\mathbf{n} - \mathbf{v}_0 \quad \text{and} \\
\eta \mathbf{t} &= \left(\mathbf{n} \cdot \mathbf{v}_0 - \sqrt{(\mathbf{n} \cdot \mathbf{v}_0)^2 + \eta^2 - 1} \right) \mathbf{n} - \mathbf{v}_0,
\end{aligned}
$$

respectively. The transformation from the normal to the reflected vector corresponds to a change of coordinates $(x_a, y_a) \to (x, y)$, where

$$
\begin{aligned}
x &= 2(\sqrt{1 - \mu_0^2}\, x_a + \mu_0 \sqrt{1 - x_a^2 - y_a^2})x_a - \sqrt{1 - \mu_0^2} \\
y &= 2(\sqrt{1 - \mu_0^2}\, x_a + \mu_0 \sqrt{1 - x_a^2 - y_a^2})y_a.
\end{aligned}
$$

The Jacobian of this change of coordinates at $(x_a, y_a) = (0, 0)$ is easily calculated to be equal to:

$$J = \begin{vmatrix} \frac{\partial x}{\partial x_a} & \frac{\partial x}{\partial y_a} \\ \frac{\partial y}{\partial x_a} & \frac{\partial y}{\partial y_a} \end{vmatrix} = \begin{vmatrix} 2\,\mu_0 & 0 \\ 0 & 2\,\mu_0 \end{vmatrix} = 4\,\mu_0^2.$$

Therefore, $\mu_0 \, d\omega = dxdy = 4\mu_0^2 dx_a dy_a = 4\mu_0^2 d\omega_a$. In other words, $d\omega = 4\mu_0 \, d\omega_a$.

The Jacobian of the change of coordinates corresponding to the refraction at $(0, 0)$ is equal to

$$\eta^2 J = \begin{vmatrix} \mu_0 - \mu_t & 0 \\ 0 & \mu_0 - \mu_t \end{vmatrix} = (\mu_0 - \mu_t)^2,$$

where $\mu_t = \sqrt{\mu_0^2 + \eta^2 - 1}$ is the cosine of the refracted direction. Again we have the chain of relations

$$\frac{1}{\eta}\mu_t \, d\omega = dxdy = \frac{1}{\eta^2}(\mu_0 - \mu_t)^2 \, dx_a dy_a = \frac{1}{\eta^2}(\mu_0 - \mu_t)^2 \, d\omega_a.$$

Therefore, $d\omega = (\mu_0^2 - \mu_t)^2 (\eta \mu_t)^{-1} \, d\omega_a$.

C Representation of the Phase Function

The Henyey-Greenstein Phase function has the nice property that it can be expanded explicitly in a cosine series given by Equation 18. The coefficients in the expansion are expressed in terms of the associated Legendre functions [3]. This explains why this phase function is so popular in the radiative transfer literature. The expansion follows from the following result [6]:

$$p(\cos\gamma) = \sum_{k=0}^{N} (2k+1)g^k P_k(\cos\gamma),$$

where P_k is the Legendre polynomial of degree k. From a well known relation between the Legendre polynomials and the associated ones[2], we see that the coefficients in the expansion of Equation 18 are given by:

$$p_k(\mu',\mu) = (2 - \delta_{0,k}) \sum_{n=k}^{N} (2n+1)g^n \frac{(n-k)!}{(n+k)!} P_n^k(\mu') P_n^k(\mu).$$

D Discrete Representation of the BRDF and BTDF

Let $\rho(\omega',\omega)$ be one of our BRDFs or BTDFs. We then want to compute the coefficients ρ_k in the cosine series:

$$\rho(\omega',\omega) = \sum_{k=0}^{N} \rho_k(\mu',\mu) \cos k(\phi - \phi').$$

Unlike the phase function in Appendix C, we cannot express these coefficients analytically for the BRDF and BTDF derived in Section 4. For the given set of ordinates $\mu_1, \cdots, \mu_M$ we approximate the integrals:

$$I_k(\mu_n,\mu_m) = \int_0^{2\pi} \rho(\pm\mu_n, 0; \pm\mu_m, \phi) \, \cos k\phi \, d\phi,$$

for $k = 0, \cdots, N$ and $n, m = 1, \cdots, M$. The signs in the integrand depend on the BRDF/BTDF being computed. The discrete representation of the linear operators associated with ρ are then given by matrices $\mathbf{L}_k$ whose elements are

$$(L_k)_{n,m} = I_k(\mu_n,\mu_m).$$

References

1. P. Beckmann and A. Spizzichino. *The Scattering of Electromagnetic Waves from Rough Surfaces*. Pergamon, New York, 1963.
2. M. Born and E. Wolf. *Principles of Optics. Sixth (corrected) Edition*. Cambridge University Press, Cambridge, U.K., 1997.
3. S. Chandrasekhar. *Radiative Transfer*. Dover, New York, 1960.
4. R. L. Cook and K. E. Torrance. A Reflectance Model for Computer Graphics. *ACM Computer Graphics (SIGGRAPH '81)*, 15(3):307–316, August 1981.

[2]This relation was used in [10], for example.

5. P. Hanrahan and W. Krueger. Reflection from Layered Surfaces due to Subsurface Scattering. In *Proceedings of SIGGRAPH '93*, pages 165–174. Addison-Wesley Publishing Company, August 1993.

6. J. E. Hansen and L. D. Travis. Light Scattering in Planetary Atmospheres. *Space Science Reviews*, 16:527–610, 1974.

7. X. D. He. *Physically-Based Models for the Reflection, Transmission and Subsurface Scattering of Light by Smooth and Rough Surfaces, with Applications to Realistic Image Synthesis.* PhD thesis, Cornell University, Ithaca, New York, 1993.

8. H. W. Jensen, S. R. Marschner, M. Levoy, and P. Hanrahan. A Practical Model for Subsurface Light Transport. In *Computer Graphics Proceedings, Annual Conference Series, 2001*, page (to appear), August 2001.

9. Z. Jin and K. Stamnes. Radiative transfer in nonuniformly refracting layered media: atmosphere-ocean system. *Applied Optics*, 33(3):431–442, January 1994.

10. J. T. Kajiya and B. P. von Herzen. Ray Tracing Volume Densities. *ACM Computer Graphics (SIGGRAPH '84)*, 18(3):165–174, July 1984.

11. E. P. F. Lafortune, S-C. Foo, K. E. Torrance, and D. P. Greenberg. Non-Linear Approximation of Reflectance Functions. In *Computer Graphics Proceedings, Annual Conference Series, 1997*, pages 117–126, August 1997.

12. E. Languénou, K.Bouatouch, and M.Chelle. Global illumination in presence of participating media with general properties. In *Proceedings of the 5th Eurographics Workshop on Rendering*, pages 69–85, Darmstadt, Germany, June 1994.

13. S. R. Marschner, S. H. Westin, E. P. F. Lafortune, K. E. Torrance, and D. P. Greenberg. Image-based brdf measurement including human skin. *Eurographics Workshop on Rendering*, 1999.

14. N. Max. Efficient light propagation for multiple anisotropic volume scattering. In *Proceedings of the 5th Eurographics Workshop on Rendering*, pages 87–104, Darmstadt, Germany, June 1994.

15. C. D. Mobley. A numerical model for the computation of radiance distributions in natural waters with wind-roughened surfaces. *Limnology and Oceanography*, 34(8):1473–1483, 1989.

16. S. K. Nayar, K. Ikeuchi, and T. Kanade. Surface Reflection: Physical and Geometrical Perspectives. *IEEE Transactions on Pattern Analysis and Machine Intelligence*, 13(7):611–634, July 1991.

17. NETLIB. The code is publicly available from `http://netlib.org`.

18. M. Pharr and P. Hanrahan. Monte Carlo Evaluation of Non-Linear Scattering Equations for Subsurface Reflection. In *Computer Graphics Proceedings, Annual Conference Series, 2000*, pages 75–84, July 2000.

19. G. N. Plass, G. W. Kattawar, and F. E. Catchings. Matrix operator theory of radiative transfer. 1: Rayleigh scattering. *Applied Optics*, 12(2):314–329, February 1973.

20. A. A. Prahl, M. J. C. van Gemert, , and A. J. Welch. Determining the optical properties of turbid media by using the adding-doubling method. *Applied Optics*, 32:559–568, 1993.

21. K. Stamnes and P. Conklin. A New Multi-Layer Discrete Ordinate Approach to Radiative Transfer in Vertically Inhomogeneous Atmospheres. *Journal of Quantum Spectroscopy and Radiative Transfer*, 31(3):273–282, 1984.

22. K. E. Torrance and E. M. Sparrow. Theory for Off-Specular Reflection From Roughened Surfaces. *Journal of the Optical Society of America*, 57(9):1105–1114, September 1967.

23. V. V. Tuchin. Light scattering study of tissue. *Physics - Uspekhi*, 40(5):495–515, 1997.

24. M. J. C. van Gemert, S. L. Jacques, H. J. C. M. Sterenborg, and W. M. Star. Skin optics. *IEEE Transactions on Biomedical Engineering*, 36(12):1146–1154, December 1989.

25. B. van Ginneken, M. Stavridi, and J. J. Koenderink. Diffuse and specular reflectance from rough surfaces. *Applied Optics*, 37(1):130–139, January 1998.

(a) Comparison of our shader (right) with a Lambertian shader(left) and the Hanrahan-Krueger model (center)
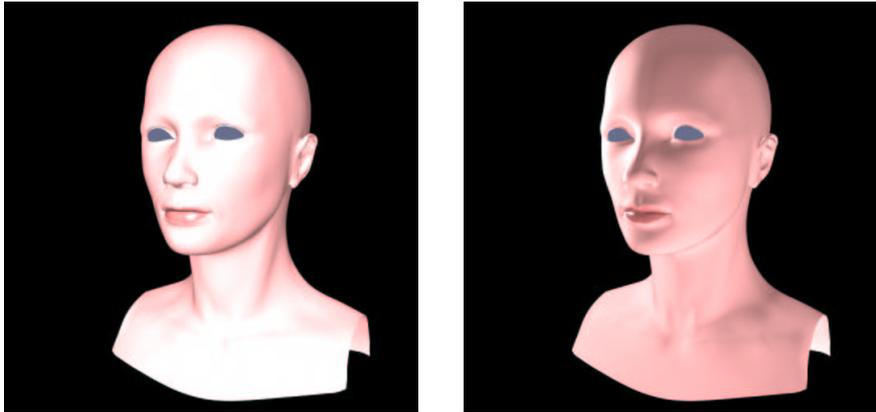
(b) Head under different lighting conditions. Flash-like area source (left) and two area light sources (right)
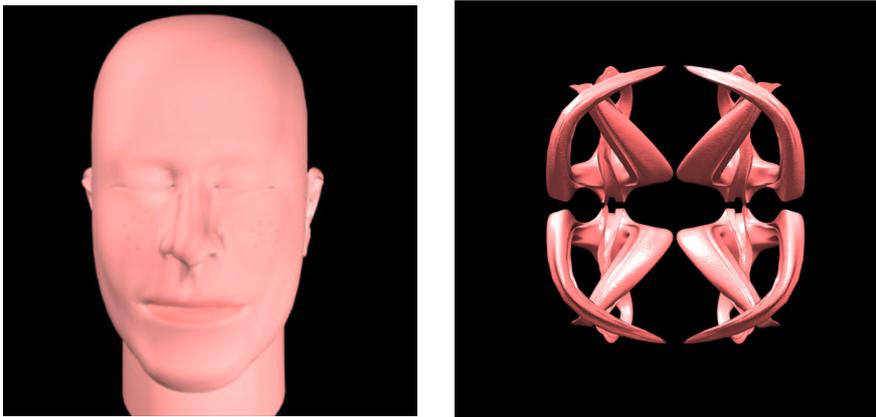
(c) Another head model with lips and freckles texture mapped.

(d) Another application of our model.

Fig. 6. Renderings created using our new skin shader.